ADVANCED ELECTRONIC MATERIALS
www.advelectronicmat.de

Unprecedentedly Wide Curie-Temperature Windows as Phase-Transition Design Platform for Tunable Magneto-Multifunctional Materials

Zhi-Yang Wei, En-Ke Liu, Yong Li, Gui-Zhou Xu, Xiao-Ming Zhang, Guo-Dong Liu, Xue-Kui Xi, Hong-Wei Zhang, Wen-Hong Wang,* Guang-Heng Wu, and Xi-Xiang Zhang*

A coupling of ferroelasticity and ferromagnetism[1,2] can lead to a multiferroic behavior of first-order magnetostructural phase transition (MST) in magnetoelastic materials. Attractive physical effects, such as ferromagnetic shape memory,[3] magnetostrain,[4] magnetocaloric effect (MCE),[5,6] magnetoresistance,[7] and exchange bias,[8] are observed based on the MSTs. These effects are receiving increasing attentions from the applications in actuating,[9] sensing,[10] magnetic cooling,[11] heat pump,[12] and energy conversion.[13] As an important class of MSTs, ferromagnetic martensitic transformations (FMMTs) are widely found in Heusler, Fe-based, and MM′X alloys, and produce diversiform physical discontinuities due to the significant alterations in crystallographic, electronic, orbital, and magnetic structures in the systems. Extraordinary magneto-multifunctional properties emerge thereby and can be tuned in different ways.

Profiting from FMMTs, the magnetic-field-induced shape memory effect and giant magnetostrain/magnetostriction have been extensively studied with promising potential in micromechanical controls and strain outputs. The MCE,[14] which happens in a magnetic transition, can be enhanced appreciably by first-order FMMTs with great changes in structural entropy in spin-lattice coupled systems.[15–17] Materials bearing FMMTs are thus further considered as candidates for caloric applications, probably combined with mechanocaloric or electrocaloric effects.[18,19] Very recently, an inspiring application of electric power generation,[20,21] using first-order FMMT ferromagnets driven by high-temperature heat resources, becomes increasingly attractive for the energy conversion, which demonstrates an exciting advance in magneto-multifunctionalities of magnetoelastic alloys.

For all the magneto-multifunctionalities, the magnetostructural coupling plays a fundamental role, since only in this case can the structural and magnetic transitions modulate each other. In order to approach FMMTs, the martensitic transformations should happen below the Curie temperature (T_C) of the system so that they couple with magnetic state changes. Along with the increasing demands of diversified functional applications, searching for new materials with highly tunable FMMTs, especially in a much wider working temperature range, is ever growing. However, challenges exist in practice. One challenge is to enlarge the magnetization change (ΔM) across FMMTs to maximize the magnetic-energy change especially in a moderate magnetic field. The other challenge is to broaden the temperature range where the FMMTs can take place, similar to the case in magnetocaloric materials Gd-Si-Ge between 20 and 290 K,[23] or the case in Mn-Fe-P-As between 150 and 350 K.[24] For first-order FMMTs, the structural transitions are often limited in a temperature range between just above room temperature and liquid-nitrogen temperature. If T_C of an FMMT material could be tailored to higher temperatures, the temperature space in which magnetostructural coupling can occur will be expanded largely.

As a rising family of FMMT materials, the hexagonal MM′X (M, M′ = transition metals, X = carbon or boron group elements) compounds have been intensively studied in recent years.[25–27] The FMMTs in these compounds are characterized by small thermal hysteresis, high temperature-sensitivity, high Curie-temperatures, gigantic anisotropic strains, huge volume expansions, large magnetization jump, magnetic-field-induced shape memory effects, and giant MCEs,[26,28–30] which collectively make MM′X compounds rather different from the conventional FMMT materials (for example, Heusler alloys). Many methods, including physical pressure, chemical modification, atom-vacancy introducing, and quench-relaxation annealing, have been adopted to tune the FMMTs. In our previous works,[26,29] we proposed an isostructural alloying principle to guide the chemical substitution during the material design. On this principle, we alloyed two isostructural compounds that have the same crystal structure but distinct phase stability and different magnetic behaviors together to form a new compound, by which we were able to manipulate both the phase transition and the magnetic exchange interactions simultaneously in a

Z.-Y. Wei, Dr. E.-K. Liu, Y. Li, G.-Z. Xu, X.-M. Zhang, Dr. X.-K. Xi, Dr. H.-W. Zhang, Dr. W.-H. Wang, Prof. G.-H. Wu
State Key Laboratory for Magnetism
Beijing National Laboratory for Condensed Matter Physics
Institute of Physics
Chinese Academy of Sciences
Beijing 100190, P. R. China
E-mail: ekliu@iphy.ac.cn; wenhong.wang@iphy.ac.cn
Y. Li, Prof. G.-D. Liu
School of Materials Science and Engineering
Hebei University of Technology
Tianjin 300130, China
Prof. X.-X. Zhang
Division of Physical Science and Engineering
King Abdullah University of Science and Technology
Thuwal 23955-6900, Saudi Arabia

DOI: 10.1002/aelm.201500076

ADVANCED ELECTRONIC MATERIALS
www.advelectronicmat.de

www.MaterialsViews.com

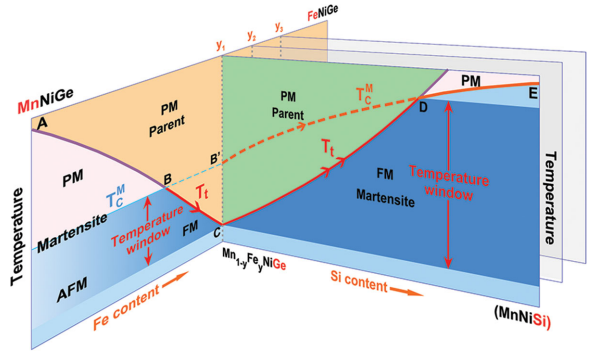

Scheme 1. A schematic of the alloy design indicated by the structural and magnetic phase diagram for MnNiGe-FeNiGe ($Mn_{1-y}Fe_yNiGe$) isostructural system (left) and $Mn_{1-y}Fe_yNiGe$-MnNiSi ($Mn_{1-y}Fe_yNiGe_{1-x}Si_x$ termed as (y, x)) one (right). Curve ABC represents T_t curve of martensitic structural transition from Ni_2In-type hexagonal parent phase to TiNiSi-type orthorhombic martensite. T_t curve crosses Curie-temperature curve (T_C^M) of martensite at point B and magnetic ordering temperature (T_g^A) of austenite at point C. Between T_C^M and T_g^A (points B and C), a Curie-temperature window (CTW) and tunable PM-FM-type FMMTs were realized by Liu et al.[26] Right part of the schematic shows the desired phase diagram in this study produced by isostructurally alloying $Mn_{1-y}Fe_yNiGe$ with MnNiSi. In this phase diagram, T_t and T_C^M are simultaneously expected to increase and cross over (point D) at high temperatures. A much wider CTW (between points C and D) is highly desired. Various Fe content (y_1, y_2,...) corresponds to a series of expected phase diagrams and CTWs.

material host. Recently, this effective principle has generated active influences on design and realization of the desired MST materials.[30–36]

In the light of this principle, in our previous work[26] we have alloyed MnNiGe with isostructural FeNiGe ($Mn_{1-y}Fe_yNiGe$) and established a stable magnetostructural coupling in a broad Curie-temperature window (CTW), as illustrated in left diagram in **Scheme 1**, in which tunable large MCEs have been obtained. Upon increasing Fe content (y), T_t of FMMT was efficiently lowered below T_C^M of martensite (point B in Scheme 1) and was continuously decreased down to the magnetic-frozen temperature (T_g^A, point C in Scheme 1) of the spin-glass-like austenite. Simultaneously, for martensite phase introducing of Fe atom gradually converted the spirally antiferromagnetic (AFM) coupling to ferromagnetic (FM) one, with T_N^M becoming T_C^M, and finally resulted in a high magnetization when $y > 0.22$ (near point C at $y_1 = 0.26$, deep blue region in the left diagram in Scheme 1). As a result, a CTW was established between $T_C^M \approx 350$ K and $T_g^A \approx 70$ K. In the CTW, the strong ferromagnetism of martensite, featured by decreasing saturation field (H_S) and increasing saturation magnetization (M_S), shows a positive correlation with Fe content. This work[26] provides a fundamental understanding on the tuning of magnetostructural coupling under the isostructural alloying principle and opens up a way to explore large CTWs for strongly coupled MST materials.

In this work, in line with the important success mentioned above, we design new material systems step by step by taking the strategy shown in Scheme 1. If one keeps the strong ferromagnetism around point C, at the same time tailors the transition (T_t) to high temperatures, one may obtain a series of strongly coupled MSTs with low-field effects and large ΔM. T_C^M, which determines the upper critical temperature (T_{cr}^{up}, point D) of the CTW, should be simultaneously raised from point B′ to high temperatures. By achieving this, abundant magneto-multifunctional applications can be expanded and promoted freely over a very broad temperature range from cryogenic to high temperatures.

According to the isostructural alloying principle, to realize the above purposes the isostructural counterpart to $Mn_{1-y}Fe_yNiGe$ system must meet three conditions: (1) A high T_t, which allows us to tailor the FMMT (T_t) of the alloyed system from low to high temperatures; (2) A high T_C^M, to upraise the T_{cr}^{up} of CTW; (3) A strong ferromagnetic coupling in martensite phase, to gain large ΔM, low H_S and desired magneto-multifunctional effects. Among Ni_2In-type hexagonal compounds, MnNiSi can be identified as a promising isostructural counterpart. Both its T_t and T_C^M are as high as 1200 and 600 K, respectively.[37,38] Its martensite phase is a strong ferromagnet with a low H_S and a large M_S. The high T_t hopefully drives up the FMMT from point C (Scheme 1) continuously to high temperatures with increasing alloying level of Si content (x) (red line with dual-arrows, Scheme 1). Similarly, T_C^M may be upraised as well. It is desirable that T_t and T_C^M curves would cross over at high temperatures, resulting in a brand-new CTW between two far-apart points C and D.

After determining the isostructural counterpart MnNiSi, $Mn_{0.74}Fe_{0.26}NiGe$ was taken as the first starting alloy. For MnNiSi, we just alloyed it with $Mn_{0.74}Fe_{0.26}NiGe$ by simply substituting Ge for Si atoms. An isostructural system of $Mn_{0.74}Fe_{0.26}NiGe_{1-x}Si_x$ was created. Although the FMMTs vanish in $Mn_{1-y}Fe_yNiGe$ compounds when $y > 0.26$ (for example, $y = 0.36$, 0.46, 0.55), these compositions were further taken as our starting alloys, with a consideration that an intrinsic strong ferromagnetism can be expected owing to the ferromagnetic coupling between Fe–Mn atoms in the martensite form.[26] In this work, dual-variable $Mn_{1-y}Fe_yNiGe_{1-x}Si_x$ ($y = 0.26$, 0.36, 0.46, 0.55; $0 \le x \le 1$) systems were studied systematically. A crystallographic and magnetic phase diagram was proposed in **Figure 1**a,b, based on the data from the structural (x-ray diffraction (XRD)), magnetic (M(T) curve), and thermal (differential scanning calorimetry (DSC)) measurements (more data in Supporting Information, Figures S1, S3, S5, and S6).

The alloy series of ($y = 0.26$, x) is taken as an example (Figure 1a). Upon introducing Si atoms on Ge sites, T_t begins to increase from low temperature of 74 K for $x = 0$ to high temperature up to 1000 K for $x = 1.0$, which is very close to T_t (≈1200 K) of stoichiometric MnNiSi.[37] Meanwhile, T_C^M is also increased, indicating Si substitution results in a significant enhancement in magnetic exchange interactions between Mn/Fe–Mn/Fe atoms in martensite phase. One can further see that the slope of T_t-(Si) x curve is much larger than that of T_C^M-(Si) x one. This implies that the Si substitution imposes more influence on the structural transition than on the magnetic coupling. The crossover point D mentioned in Scheme 1 appears at 434 K, which is much higher than T_C^M (350 K) of starting alloy $Mn_{1-y}Fe_yNiGe$.[26] For higher Fe contents ($y = 0.36$, 0.46, 0.55), a similar behavior is observed. Both T_t and T_C^M are simultaneously raised to high temperatures simply by Si substitution and the crossover points are thus obtained above 400 K.

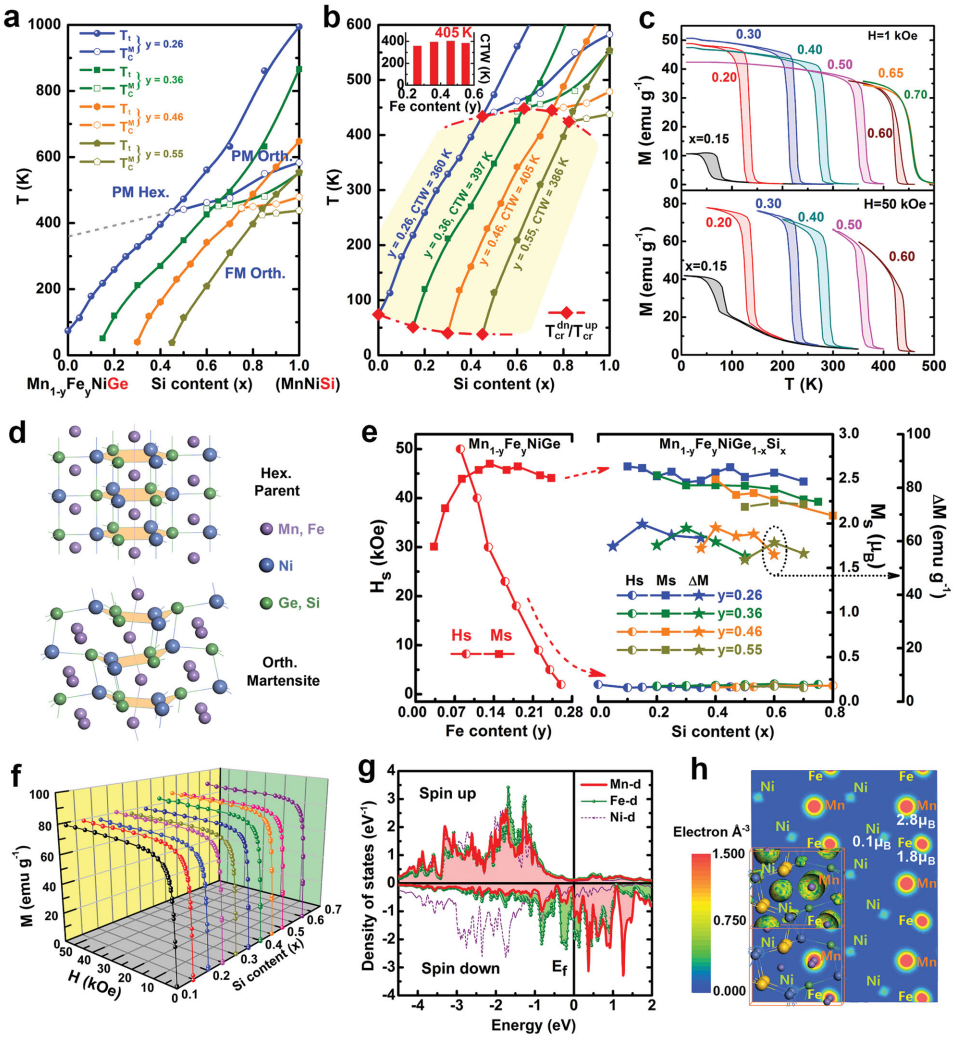

Figure 1. a) Structural and magnetic phase diagram of $Mn_{1-y}Fe_yNiGe_{1-x}Si_x$ (y, x) system. b) CTWs constructed by different Fe and Si contents. Inset shows the Fe-content (y) dependence of CTW width. Red diamond symbol denotes the upper and lower critical temperatures (T_{cr}^{up}/T_{cr}^{dn}) of CTWs. c) Thermomagnetic curves of ($y = 0.36$, x) series in magnetic field of 1 kOe (upper panel) and 50 kOe (lower panel). d) Martensitic structural transition from hexagonal parent phase to orthorhombic martensite. e) Saturation field and saturation magnetization of $Mn_{1-y}Fe_yNiGe$ (left panel, data from ref.[26] and saturation field, saturation magnetization, and magnetization difference (ΔM) across the FMMTs (right panel). f) Si-content (x) dependence of isothermal magnetization curves at 5 K for ($y = 0.26$, x) series. g) Partial density of states (PDOS) and h) contours of spin electron density of ($y = 0.5$, $x = 0.5$) alloy.

An amplified phase diagram is depicted in Figure 1b. For the alloy series of ($y = 0.26$, x), a CTW with a width of 360 K between the lower critical temperature (T_{cr}^{dn}) = 74 K and T_{cr}^{up} = 434 K is obtained. From Figure 1b, one sees that T_{cr}^{up} (crossover point) goes along a kappa-like curve with a maximum value 448 K in ($y = 0.46$, x) series, while with increasing Si content T_{cr}^{dn} further decreases from 74 K to about 38 K. These T_{cr}^{dn}, below which the displacements of alloy atoms will be frozen, are the lowest transition temperatures reported in first-order FMMT systems. As an important result, a series of unprecedentedly wide CTWs with a maximal width of 405 K between T_{cr}^{dn} and T_{cr}^{up} are obtained in $Mn_{1-y}Fe_yNiGe_{1-x}Si_x$ system (also see inset to Figure 1b). These CTWs span from below liquid nitrogen temperature (≈38 K) to room temperature and to the highest temperature of 448 K, which are much wider than the temperature distribution ranges of many other FMMTs.[17,22–24,27–31,33–36] This is the first realization that highly tunable MSTs can be gained in such wide temperature range in one material system. A strong magnetostructural coupling of ferroelasticity and ferromagnetism in $Mn_{1-y}Fe_yNiGe_{1-x}Si_x$ system is thus obtained over a quite large range, connecting the ultralow and the high temperatures. In Figure 1b, between the window boundaries (T_{cr}^{dn}-T_{cr}^{up}) (the light-yellow region), the strongly coupled MSTs can be obtained in any composition point with random (y, x) values.

The MST behaviors within the CTWs are presented by magnetization measurements. Figure 1c shows the thermomagnetic M(T) curves of ($y = 0.36$, x) alloy series (more data in Supporting Information, Figure S3). The M(T) curves with abrupt magnetization jump from paramagnetic (PM) state to

FM one, and clear but small thermal hysteresis demonstrate the first-order FMMT behavior between $0.15 \le x \le 0.60$. During the Si substitution, the FMMT can be tailored from 51 K to high temperatures, showing a high tunability. These transitions involve two structures, Ni_2In-type hexagonal parent phase and TiNiSi-type orthorhombic martensite, as illustrated in Figure 1d (see structural analysis by XRD in Supporting Information, Figure S1). The FMMT occurs from the parent phase to the martensite via distortions of Ni-Ge/Si hexagonal rings and Mn/Fe–Mn/Fe zigzag chains, with a giant volume expansion of around 3% (more data in Supporting Information, Figure S2 and Table S1). Based on this structural transition, a high temperature-sensitivity and a large magnetization jump can be observed. Furthermore, very high magnetizations are seen even in a low field of 1 kOe. Large ΔMs across the FMMTs up to 65 emu g^{-1} are measured in the CTW, as shown in Figure 1e (more data in Supporting Information, Table S2). These ideal features will promote the magneto-multifunctional properties such as giant MCEs and electric power generation at low fields with low energy consumptions, especially in a wide temperature range including the important high-temperature region. For higher Si substitution with $x = 0.65$ and 0.70, the thermal hysteresis becomes zero in the M(T) curves as the MST decouples above the upper critical temperature ($T_{cr}^{up} = 448$ K).

In order to understand the origin of ferromagnetism in martensite phase, the magnetizing behaviors at 5 K of $Mn_{1-y}Fe_yNiGe_{1-x}Si_x$ were analyzed. Here we first look back the magnetic properties of $Mn_{1-y}Fe_yNiGe$.[26] As shown in the left part of Figure 1e, M_S increases to a plateau with a value of about 2.65 μ_B upon increasing Fe content (y). Fe substitution can efficiently convert AFM couplings in MnNiGe to FM ones. H_S decreases monotonically and reaches a minimum of 5 kOe at $y = 0.24$ where the AFM coupling is almost overcome by FM couplings. In $Mn_{1-y}Fe_yNiGe$ system, the high magnetizations and low saturation fields are achieved gradually with increasing Fe substitution. After introducing Si at Ge site, in sharp contrast, the $Mn_{1-y}Fe_yNiGe_{1-x}Si_x$ ($y = 0.26$, 0.36, 0.46, 0.55) coheres the lowest H_S and highest M_S of $Mn_{1-y}Fe_yNiGe$ system and maintains them at values of $H_S \approx 1.35$ to 2.12 kOe and $M_S \approx 2.2$ to 2.6 μ_B. M(H) curves of ($y = 0.26$, x) ($0.10 \le x \le 0.60$) series are given in Figure 1f (more data in Supporting Information, Figure S4). One can see all samples are easily magnetized in a low magnetic field and gain large saturation magnetizations of about 80 emu g^{-1} (2.6 μ_B). The features of low H_S and high M_S in $Mn_{1-y}Fe_yNiGe_{1-x}Si_x$ are highly expected to facilitate the magneto-multifunctional properties, especially the desired low-field effects.

The magnetic structure in martensite phase of $Mn_{1-y}Fe_yNiGe_{1-x}Si_x$ system was further revealed by first-principles calculations. Figure 1g shows the partial density of states (PDOS) of 3*d*-metal atoms in ($y = 0.5$, $x = 0.5$) alloy, from which one sees the remarkable spin polarizations on both Mn and Fe atoms. This accounts for the large magnetic moments of ≈2.8 μ_B and ≈1.8 μ_B on Mn and Fe atoms, respectively (Supporting Information, Table S3). Compared with Mn atom, Fe atom has a weaker polarization and a clear PDOS peak exists well below the Fermi level in spin-down state, which results in a smaller moment on Fe atom. Ni and Ge/Si atoms carry near-zero moments (Supporting Information, Table S3) as the spin polarizations are very weak due to strong covalent bonds between Ni–Si/Ge atoms. Figure 1h depicts the spin electron density of sample ($y = 0.5$, $x = 0.5$), which shows the magnetization distribution in the compound. Strong localization of (positive) spin electron density values exist around both Mn/Fe atoms, indicating significant localized moments with a parallel alignment in the zigzag chains. In $Mn_{1-y}Fe_yNiGe_{1-x}Si_x$, the magnetizations, mainly originating from Mn and Fe moments with FM exchange interactions, keep high and stable values during the whole Si substitution.

In this section, we present the desired magnetic functional properties in CTWs. Isothermal M(H) curves across the FMMT of sample ($y = 0.26$, $x = 0.30$) were measured (**Figure 2**a). As illustrated, a metamagnetic behavior is observed between 338 K with a critical field (H_{cr}) of about 35 kOe and 332 K with a rather low H_{cr} of 5 kOe. This metamagnetic behavior indicates the magnetic-field-induced martensitic structural transition from PM hexagonal parent phase to an energy-favored FM orthorhombic martensite. We further characterized the MCEs upon this FMMT. The magnetic entropy changes (ΔS_m) of ($y = 0.26$, $x = 0.30$) alloy were derived from the loop-measured M(H) curves using Maxwell relation (see the Experimental Section). As shown in Figure 2b, a value of $\Delta S_m = -37$ J kg^{-1} K^{-1} was obtained at a field change $\Delta H = 50$ kOe and T = 335 K, showing a giant conventional (negative) MCE. Noticeably, the alloy shows a giant ΔS_m of –17 J kg^{-1} K^{-1} at moderate $\Delta H = 20$ kOe and T = 333 K. These giant MCEs are benefited from the abrupt and large magnetization changes during the FMMTs as well as the low H_S as discussed above.

To systematically study the dependence of MCE on the composition, we chose alloys with ($y = 0.36$, $x = 0.2$, 0.3, 0.4, 0.5, 0.6) in the CTW to perform the isothermal M(H) curves and calculated the corresponding ΔS_m, as shown in Figure 2c. It is evident that $\Delta S_m(x)$ depends on temperature very weakly in the temperature range between 120 and 440 K, and takes a value of –30 J kg^{-1} K^{-1} at $\Delta H = 50$ kOe, and a value of –12 J kg^{-1} K^{-1} at moderate $\Delta H = 20$ kOe. High-temperature giant MCEs are clearly obtained in these materials. Such large MCEs are rarely found above water boiling point (see ref. 39–41). It is important to note that these giant MCEs spanning the whole CTWs are composed of the caloric effects from both the structural and magnetic transitions and more importantly two caloric effects are locked in the same sign owing to the concurrent breaking in crystallographic and magnetic symmetries. This locked effect would greatly enhance the total caloric outcome of strongly coupled MSTs.[6,29]

To clearly present the dependence of maximum of $-\Delta S_m$ on the ΔH, we re-plotted those values of Figure 2c in Figure 2d with the corresponding fitting curves. A linear relationship between maximum of $-\Delta S_m$ and ΔH is clearly observed up to $\Delta H = 50$ kOe. This indicates that the temperature dependence of magnetization across the FMMTs is field independent,[42] which may be attributed to the specific characteristics of the fist-order transitions in these materials. The data in Figure 2d can be fitted to a linear dependence, $-\Delta S_m = \kappa \Delta H$, where the coefficient κ can be considered as the factor that describes how strong the maximum of $-\Delta S_m$ depends on ΔH. The values of κ obtained from fitting are plotted in Figure 2e, as a function of x, with the integrated refrigerant capacity (RC) that measures

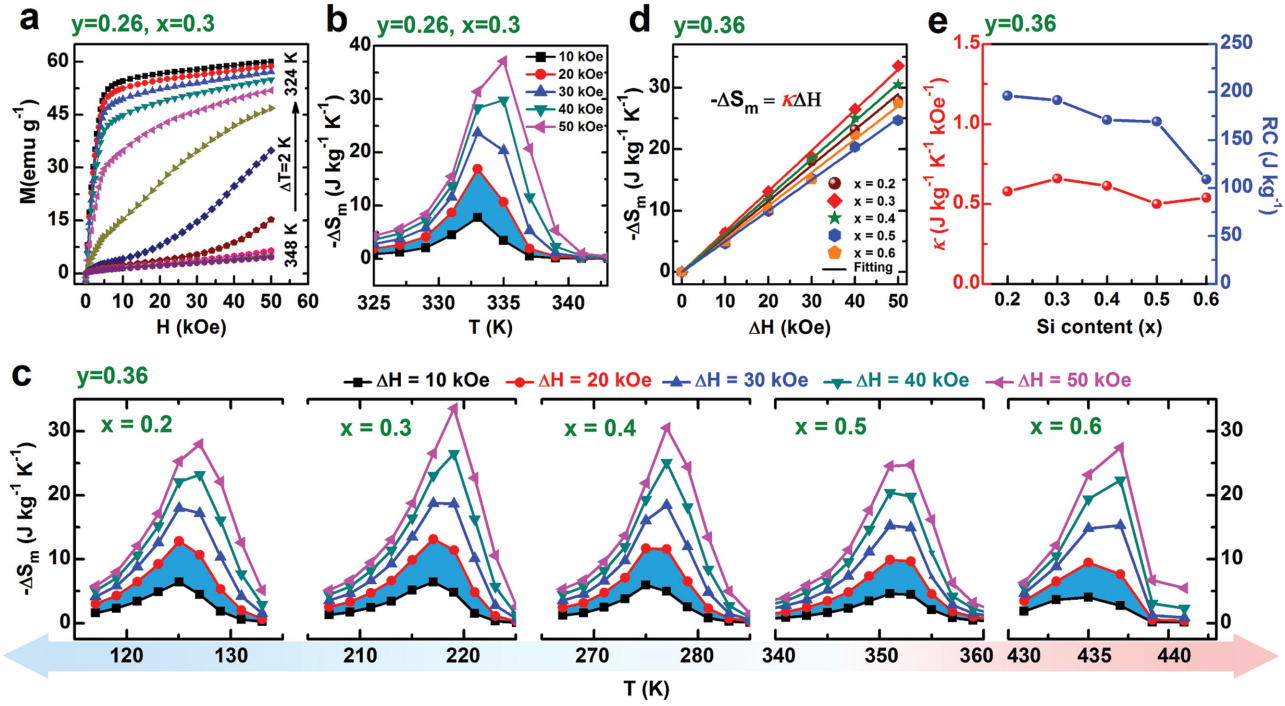

Figure 2. a) Magnetic isotherms of alloy ($\gamma = 0.26$, $x = 0.3$) at various temperatures around T_t. b) Isothermal magnetic entropy changes (ΔS_m) of alloy ($\gamma = 0.26$, $x = 0.3$). c) Isothermal magnetic entropy changes (ΔS_m) of ($\gamma = 0.36$, x) series. d) Maximum of ΔS_m for ($\gamma = 0.36$, x) series as a function of magnetic field change (ΔH). Symbols refer to experiment data and the corresponding linear fitting is shown as well. Fitting formula is $-\Delta S_m = \kappa \Delta H$. e) Si-content dependence (x) of κ and refrigerant capacity (RC) of ($\gamma = 0.36$, x) series.

the effectiveness of a magnetic refrigerant. The high values of κ and RC obtained on ($\gamma = 0.36$, x) series as shown in Figure 2e, indicate clearly the large MCEs throughout the wide CTWs.

As well known, the functional fatigue behavior is critical for practical phase-transition-based applications.[43,44] In order to investigate the fatigue characteristics on the FMMTs, thermal cycling tests were performed on DSC for some compositions of ($\gamma = 0.26$, $x = 0.15$, 0.25) and ($\gamma = 0.36$, $x = 0.60$). **Figure 3**a,b,c shows cycle-dependent calorimetric curves of alloy ($\gamma = 0.26$, $x = 0.15$). Exothermic (endothermic) peak on cooling (heating) represents forward (reverse) martensitic transitions. During 93 cycles in this study, the transition calorimetric profiles were unchanged, particularly in the peak positions and peak heights, which demonstrate that the phase transitions

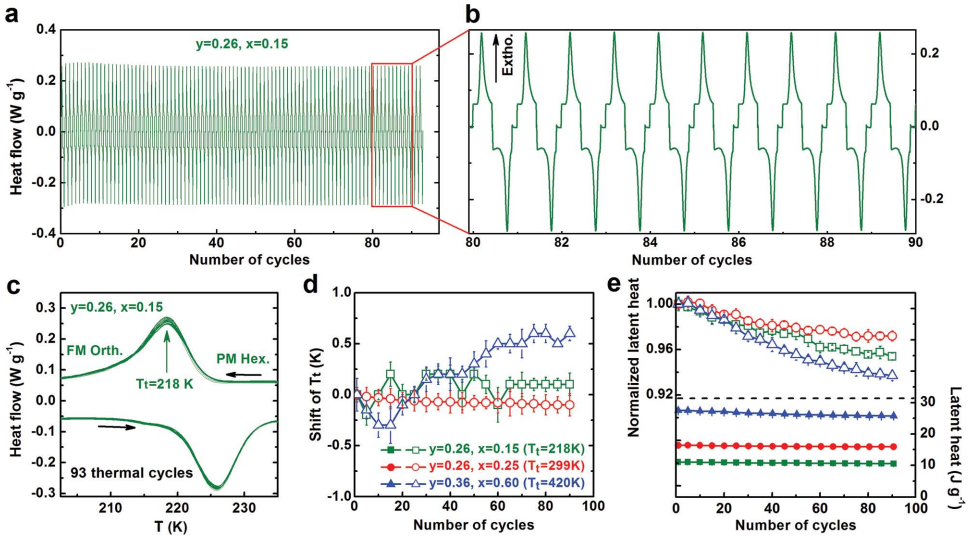

Figure 3. Functional fatigue behavior of $Mn_{1-\gamma}Fe_\gamma NiGe_{1-x}Si_x$ (γ, x) system. a–c) DSC data of thermal cycling with 93 times around T_t of alloy ($\gamma = 0.26$, $x = 0.15$). An enlarged image of cycles from 80 to 89 is shown in (b). d) Shift of T_t, e) absolute (lower panel) and normalized (upper panel) latent heats (ΔE) upon cooling of alloys ($\gamma = 0.26$, $x = 0.15$), ($\gamma = 0.26$, $x = 0.25$), and ($\gamma = 0.36$, $x = 0.60$) deprived from DSC data.

possess good reversibility and stability. The same thermal-cycling experiments were carried out on other two alloys ($\gamma = 0.26$, $x = 0.25$) and ($\gamma = 0.36$, $x = 0.60$). The associated shift of T_t, absolute and normalized latent heats (ΔE) are presented in Figure 3d,e (more data in Supporting Information, Table S4). For the transitions at low (218 K) and room (299 K) temperatures ($\gamma = 0.26$, $x = 0.15$, 0.25), T_t keeps almost unchanged throughout the whole cycling process with a small fluctuation less than 0.5 K (for sample with $x = 0.25$, the shift of $T_t \approx$ 0.1 K after 93 cycles), indicating an even better functional stability than the excellent Ni-Ti-Cu/Pd alloys.[43,44] This stability is further confirmed by a slight decay (3%–5%) in ΔE following by a saturation tendency. Even for the transitions at 420 K (147 °C) in alloy ($\gamma = 0.36$, $x = 0.60$), only very slight changes of T_t (≈0.8 K) and ΔE (≈7%) can be observed. These slightly enlarged changes may be ascribed to the atom motions by high-temperature thermal activation. It is clear that the studied alloys show a potentially robust functional stability even at high temperatures, which will benefit the multifunctional applications of the materials.

Figure 4 shows a general comparison of the maximum entropy changes ($|\Delta S|_{max}$) of our materials and several well-known MCE materials based on current statistical data (Supporting Information, Table S5). The graphic is in general consistent with the one reported by Franco et al.[14] In this graphic, low- and room-temperature MCEs are observed in many rare-earth and Mn-based compounds, including the first-order FMMT materials such as Heusler and MM′X alloys. However, the MCEs in each family (usually consist of several material members) are limited in narrow temperature spans since many MSTs can only be tuned in a limited temperature range. It can be seen that different families show their dissimilar transition temperatures but most giant MCEs occur below 370 K. In particular, the MCEs of MM′X alloys also exist mainly in a relatively narrow range around room temperature. In sharp contrast, our $Mn_{1-\gamma}Fe_\gamma NiGe_{1-x}Si_x$ single material system strikingly shows giant MCEs over the very wide temperature range from 40 to 450 K. Within these wide CTWs, the magnetostrain-based applications in forms of bulks, particles or composites can also be designed. It is further conceivable that large MCEs and barocaloric effects tuned by applying pressure[18,34] and table-like MCEs produced by composition-gradient composites[45]

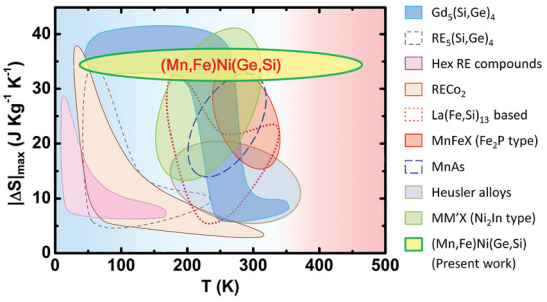

Figure 4. A statistical graphic of absolute values of maximum entropy changes ($|\Delta S|_{max}$) for ΔH = 50 kOe versus peak temperature for different families of magnetocaloric materials, including the present (Mn,Fe)Ni(Ge,Si) system. Detail data and relevant references are included in Supporting Information, Table S5. Here, RE refers to rare-earth elements, Hex to hexagonal structure, and X to *p*-block elements.

can be freely designed at any desired temperature within such broad range. In addition to the use as magnetic refrigerant, the giant MCE materials can also be applied as promising working substances for magnetic heat pumps or electric power generations.[12,20] For these applications, the MSTs are required to occur at high temperatures in order to gain the heats efficiently and cyclically from ambient environments, driven by hot water or vapor from sea surface (30–40 °C) or geothermal spring (50–100 °C), or by the exhausted heats from applications of hypercritical CO_2 (≈120 °C), automobile and industrial production (100–500 °C). For the high-temperature MSTs between 373 and 448 K, furthermore, the corresponding materials show an increasingly low cost due to the high-level Si-substitution for expensive Ge element.

In conclusion, applying the principle of isostructural alloying, we have successfully realized the strongly coupled magneto-structural transitions within a series of unprecedentedly wide Curie-temperature windows, with widths as large as 400 K, in a single host system (Mn,Fe)Ni(Ge,Si). This work reveals clear physical pictures of the tuning route in material design and the Curie-temperature windows for phase transitions. The combination of low-field large MCEs, locked caloric effects, wide working temperature, and robust functional stability makes the materials promising for various smart applications including shape-memory/strain-based output,[46] solid-state multicaloric cooling/heating,[19] and energy conversion.[20] The unprecedentedly wide Curie-temperature windows provide a broad design platform of magnetostructural transitions for tunable magneto-multifunctional properties of the rare-earth-free Mn-based (Mn,Fe)Ni(Ge,Si) multiferroic magnetoelastic alloys. The strongly coupled magnetostructural transitions can be manipulated in frameworks of compositional engineering,[29,47] pressure modulations,[18,34,48] and low-dimensional forming[4,49] for potential applications, including strain-based composites,[50,51] functional devices,[46,52] and multiferroic heterostructures.[53,54]

Experimental Section

Experimental Methods: Highly purified metals were arc-melted under argon atmosphere. Each ingot was melted for four times and was turned over after each melting process. As-cast ingots were annealed in evacuated quartz tubes filled with high-purity argon at 1123 K for 5 d and cooled down to room temperature slowly. Powder XRD analysis were performed on a Rigaku D/max 2,400 X-ray diffractometer with Cu-$K\alpha$ radiation at room temperature. Magnetic measurements including thermomagnetic curves and isothermal magnetization curve were carried out on a superconductive interference device (SQUID) magnetometer and physical property measurement system (PPMS, Quantum Design). Thermomagnetic curves with temperature above 400 K were performed on a PPMS plus vibrating sample magnetometer (VSM) with a maximum field of 50 kOe. Thermal analysis was performed using differential scanning calorimetry (DSC STA 449 F3 Jupiter and DSC 214 Ployma, NETZSCH). The ramping rate is 5 K min^{-1}. By adding an apparatus involving two permanent magnets, the gravity change caused by magnetic transition can be detected on the thermogravimetric analyzer. The magnetic entropy changes (ΔS_m) across magnetostructural transitions were derived from the magnetization curves using the Maxwell relation:[14] $\Delta S_m(T,H) = S_m(T,H) - S_m(T,0) = \int_0^H \left(\frac{\partial M}{\partial T}\right)_H dH$. The RC is defined as $RC = \int_{T_1}^{T_2} |\Delta S_m| dT$, where T_1 and T_2 are two temperatures of the half maximum of $\Delta S_m(T)$ peak.[14] To avoid fake ΔS_m

values, the temperature loop process method[55] was applied to measure the isothermal magnetization curves with an interval of 2 K for these FMMTs with a clear thermal hysteresis.

Calculation Methods: The first-principles calculations on density of states (DOS), magnetic moment distribution, and spin electron density (SED) were performed using ultrasoft pseudopotential method based on the density function theory (DFT).[56] The exchange and correlation energies were treated using the generalized gradient approximations. 500 eV cutoff-energy in the plane-wave basis and 120 *k*-points in the irreducible Brillouin zone were used for a good convergence of the total energy. The total-energy difference tolerance for the self-consistent field iteration was set at 1×10^{-6} eV per atom.

Supporting Information

Supporting Information is available from the Wiley Online Library or from the author.

Acknowledgements

This work was supported by National Natural Science Foundation of China (51301195, 11174352, and 51431009), National Basic Research Program of China (2012CB619405 and 2011CB012800), Beijing Municipal Science & Technology Commission (Z141100004214004), and Youth Innovation Promotion Association of Chinese Academy of Sciences (2013002). This article was amended on July 15, 2015 to correct the citation of ref. 39–41 on page 4.

Received: February 24, 2015
Revised: April 10, 2015
Published online: May 18, 2015

[1] W. Eerenstein, N. D. Mathur, J. F. Scott, *Nature* **2006**, *442*, 759.
[2] E. K. H. Salje, *Annu. Rev. Mater. Res.* **2012**, *42*, 265.
[3] R. Kainuma, Y. Imano, W. Ito, Y. Sutou, H. Morito, S. Okamoto, O. Kitakami, K. Oikawa, A. Fujita, T. Kanomata, K. Ishida, *Nature* **2006**, *439*, 957.
[4] M. Chmielus, X. X. Zhang, C. Witherspoon, D. C. Dunand, P. Mullner, *Nat. Mater.* **2009**, *8*, 863.
[5] T. Krenke, E. Duman, M. Acet, E. F. Wassermann, X. Moya, L. Manosa, A. Planes, *Nat. Mater.* **2005**, *4*, 450.
[6] J. Liu, T. Gottschall, K. P. Skokov, J. D. Moore, O. Gutfleisch, *Nat. Mater.* **2012**, *11*, 620.
[7] S. Singh, R. Rawat, S. E. Muthu, S. W. D'Souza, E. Suard, A. Senyshyn, S. Banik, P. Rajput, S. Bhardwaj, A. M. Awasthi, R. Ranjan, S. Arumugam, D. L. Schlagel, T. A. Lograsso, A. Chakrabarti, S. R. Barman, *Phys. Rev. Lett.* **2012**, *109*, 246601.
[8] A. K. Nayak, M. Nicklas, S. Chadov, C. Shekhar, Y. Skourski, J. Winterlik, C. Felser, *Phys. Rev. Lett.* **2013**, *110*, 127204.
[9] H. E. Karaca, I. Karaman, B. Basaran, Y. Ren, Y. I. Chumlyakov, H. J. Maier, *Adv. Funct. Mater.* **2009**, *19*, 983.
[10] N. Sarawate, M. Dapino, *Appl. Phys. Lett.* **2006**, *88*, 121923.
[11] S. Fähler, U. K. Rößler, O. Kastner, J. Eckert, G. Eggeler, H. Emmerich, P. Entel, S. Müller, E. Quandt, K. Albe, *Adv. Eng. Mater.* **2012**, *14*, 10.
[12] B. Yu, M. Liu, P. W. Egolf, A. Kitanovski, *Int. J. Refrig.* **2010**, *33*, 1029.
[13] O. Gutfleisch, M. A. Willard, E. Brück, C. H. Chen, S. G. Sankar, J. P. Liu, *Adv. Mater.* **2011**, *23*, 821.
[14] V. Franco, J. S. Blazquez, B. Ingale, A. Conde, *Annu. Rev. Mater. Res.* **2012**, *42*, 305.
[15] B. Li, W. J. Ren, Q. Zhang, X. K. Lv, X. G. Liu, H. Meng, J. Li, D. Li, Z. D. Zhang, *Appl. Phys. Lett.* **2009**, *95*, 172506.
[16] T. Kihara, X. Xu, W. Ito, R. Kainuma, M. Tokunaga, *Phys. Rev. B* **2014**, *90*, 214409.
[17] A. Planes, L. Manosa, M. Acet, *J. Phys. Condens. Matter* **2009**, *21*, 233201.
[18] L. Manosa, D. González-Alonso, A. Planes, E. Bonnot, M. Barrio, J. L. Tamarit, S. Aksoy, M. Acet, *Nat. Mater.* **2010**, *9*, 478.
[19] X. Moya, S. Kar-Narayan, N. D. Mathur, *Nat. Mater.* **2014**, *13*, 439.
[20] V. Srivastava, Y. Song, K. Bhatti, R. D. James, *Adv. Energy Mater.* **2011**, *1*, 97.
[21] Y. T. Song, K. P. Bhatti, V. Srivastava, C. Leighton, R. D. James, *Energy Environ. Sci.* **2013**, *6*, 1315.
[22] S. Y. Yu, L. Ma, G. D. Liu, Z. H. Liu, J. L. Chen, Z. X. Cao, G. H. Wu, B. Zhang, X. X. Zhang, *Appl. Phys. Lett.* **2007**, *90*, 242501.
[23] V. K. Pecharsky, K. A. Gschneidner, *Appl. Phys. Lett.* **1997**, *70*, 3299.
[24] O. Tegus, E. Bruck, L. Zhang, Dagula, K. H. J. Buschow, F. R. de Boer, *Physica B* **2002**, *319*, 174.
[25] A. Barcza, Z. Gercsi, K. S. Knight, K. G. Sandeman, *Phys. Rev. Lett.* **2010**, *104*, 247202.
[26] E. K. Liu, W. H. Wang, L. Feng, W. Zhu, G. J. Li, J. L. Chen, H. W. Zhang, G. H. Wu, C. B. Jiang, H. B. Xu, F. de Boer, *Nat. Commun.* **2012**, *3*, 873.
[27] D. Choudhury, T. Suzuki, Y. Tokura, Y. Taguchi, *Sci. Rep.* **2014**, *4*, 7544.
[28] T. Samanta, I. Dubenko, A. Quetz, S. Stadler, N. Ali, *Appl. Phys. Lett.* **2012**, *101*, 242405.
[29] E. K. Liu, H. G. Zhang, G. Z. Xu, X. M. Zhang, R. S. Ma, W. H. Wang, J. L. Chen, H. W. Zhang, G. H. Wu, L. Feng, X. X. Zhang, *Appl. Phys. Lett.* **2013**, *102*, 122405.
[30] C. L. Zhang, D. H. Wang, Z. D. Han, B. Qian, H. F. Shi, C. Zhu, J. Chen, T. Z. Wang, *Appl. Phys. Lett.* **2013**, *103*, 132411.
[31] G. J. Li, E. K. Liu, H. G. Zhang, Y. J. Zhang, J. L. Chen, W. H. Wang, H. W. Zhang, G. H. Wu, S. Y. Yu, *J. Magn. Magn. Mater.* **2013**, *332*, 146.
[32] J. H. Chen, E. K. Liu, X. Qi, H. Z. Luo, W. H. Wang, H. W. Zhang, S. G. Wang, J. W. Cai, G. H. Wu, *Comput. Mater. Sci.* **2014**, *89*, 130.
[33] L. F. Zhang, J. M. Wang, H. Hua, C. B. Jiang, H. B. Xu, *Appl. Phys. Lett.* **2014**, *105*, 112402.
[34] T. Samanta, D. L. Lepkowski, A. U. Saleheen, A. Shankar, J. Prestigiacomo, I. Dubenko, A. Quetz, I. W. H. Oswald, G. T. McCandless, J. Y. Chan, P. W. Adams, D. P. Young, N. Ali, S. Stadler, *Phys. Rev. B* **2015**, *91*, 020401.
[35] T. Samanta, D. L. Lepkowski, A. U. Saleheen, A. Shankar, J. Prestigiacomo, I. Dubenko, A. Quetz, I. W. H. Oswald, G. T. McCandless, J. Y. Chan, P. W. Adams, D. P. Young, N. Ali, S. Stadler, *J. Appl. Phys.* **2015**, *117*, 123911.
[36] C. L. Zhang, H. F. Shi, E. J. Ye, Y. G. Nie, Z. D. Han, D. H. Wang, *J. Alloys Compd.* **2015**, *639*, 36.
[37] V. Johnson, *Inorg. Chem.* **1975**, *14*, 1117.
[38] W. Bażela, A. Szytuła, J. Todorovic, A. Zieba, *Phys. Status Solidi A* **1981**, *64*, 367.
[39] V. Franco, J. S. Blázquez, C. F. Conde, A. Conde, *Appl. Phys. Lett.* **2006**, *88*, 042505.
[40] M. Jasinski, J. Liu, S. Jacobs, C. Zimm, *J. Appl. Phys.* **2010**, *107*, 09A953.
[41] W. J. Feng, Q. Zhang, L. Q. Zhang, B. Li, J. Du, Y. F. Deng, Z. D. Zhang, *Solid State Commun.* **2010**, *150*, 949.
[42] V. Franco, A. Conde, *Int. J. Refrig.* **2010**, *33*, 465.
[43] R. Zarnetta, R. Takahashi, M. L. Young, A. Savan, Y. Furuya, S. Thienhaus, B. Maaß, M. Rahim, J. Frenzel, H. Brunken, Y. S. Chu, V. Srivastava, R. D. James, I. Takeuchi, G. Eggeler, A. Ludwig, *Adv. Funct. Mater.* **2010**, *20*, 1917.
[44] Y. T. Song, X. Chen, V. Dabade, T. W. Shield, R. D. James, *Nature* **2013**, *502*, 85.
[45] L. Li, M. Kadonaga, D. Huo, Z. Qian, T. Namiki, K. Nishimura, *Appl. Phys. Lett.* **2012**, *101*, 122401.

[46] J. Liu, N. Scheerbaum, S. Kauffmann-Weiss, O. Gutfleisch, *Adv. Eng. Mater.* **2012**, *14*, 653.
[47] I. Takeuchi, O. O. Famodu, J. C. Read, M. A. Aronova, K. S. Chang, C. Craciunescu, S. E. Lofland, M. Wuttig, F. C. Wellstood, L. Knauss, A. Orozco, *Nat. Mater.* **2003**, *2*, 180.
[48] L. Caron, N. T. Trung, E. Brück, *Phys. Rev. B* **2011**, *84*, 020414.
[49] J. S. Juan, M. L. No, C. A. Schuh, *Nat. Nanotechnol.* **2009**, *4*, 415.
[50] D. C. Hofmann, *Science* **2010**, *329*, 1294.
[51] Y. Y. Zhao, F. X. Hu, L. F. Bao, J. Wang, H. Wu, Q. Z. Huang, R. R. Wu, Y. Liu, F. R. Shen, H. Kuang, M. Zhang, W. L. Zuo, X. Q. Zheng, J. R. Sun, B. G. Shen, *J. Am. Chem. Soc.* **2015**, *137*, 1746.
[52] M. Gueltig, H. Ossmer, M. Ohtsuka, H. Miki, K. Tsuchiya, T. Takagi, M. Kohl, *Adv. Energy Mater.* **2014**, *4*, 1400751.
[53] X. Moya, L. E. Hueso, F. Maccherozzi, A. I. Tovstolytkin, D. I. Podyalovskii, C. Ducati, L. C. Phillips, M. Ghidini, O. Hovorka, A. Berger, M. E. Vickers, E. Defay, S. S. Dhesi, N. D. Mathur, *Nat. Mater.* **2013**, *12*, 52.
[54] Y. Y. Gong, D. H. Wang, Q. Q. Cao, E. K. Liu, J. Liu, Y. W. Du, *Adv. Mater.* **2015**, *27*, 801.
[55] L. Caron, Z. Q. Ou, T. T. Nguyen, D. T. C. Thanh, O. Tegus, E. Brück, *J. Magn. Magn. Mater.* **2009**, *321*, 3559.
[56] M. C. Payne, M. P. Teter, D. C. Allan, T. A. Arias, J. D. Joannopoulos, *Rev. Mod. Phys.* **1992**, *64*, 1045.